Exploring the Pareto Fronts of Actuation Technologies for High Performance Mechatronic Systems

Ernst Csencsics and Georg Schitter, *Senior Member, IEEE*

***Abstract*—In the course of designing high performance mechatronic scanning systems typically several conflicting requirements, such as speed and range, must be met at the same time. Actuators are a key component in this relation, as depending on the system specifications, different actuation technologies may prove advantageous. Due to the large number of design parameters a comprehensive and general comparison of actuation technologies across various mechatronic system classes is however difficult. This paper proposes a novel method for estimating the limitations of individual actuation technologies for a desired system class based on analytically obtained relations, which can be used to systematically trade off desired range and speed specifications in the design phase. The method is presented along the example class of fast steering mirrors (FSMs) with the tradeoff limit curves (Pareto fronts) estimated for the established piezo electric, Lorentz force and hybrid reluctance actuation technologies. The classification is validated against the results of a thorough review of reported FSM system specifications. The obtained results clearly suggest that piezo actuated FSMs have smaller ranges but are superior to Lorentz force actuated FSMs for bandwidths larger than 2 kHz and ranges below 20 mrad. The estimated Pareto front for FSMs with the least common hybrid reluctance technology further suggest that this technology is superior to both of the other technologies for FSMs with a bandwidth above 700 Hz and angular ranges below 120 mrad.**

***Index Terms*—Fast steering mirror, System analysis and design, actuators**

I. Introduction

High performance mechatronic positioning and scanning systems are important and performance determining components of many scientific instruments, measurement and production systems. Typical examples for systems integrating such scanning units include optical lithography machines for the semiconductor industry [1], [2], atomic force microscopes (AFMs) [3], [4], laser scanning microscopes [5], [6] or optical 3D sensor systems [7], [8]. These positioning and scanning systems are in general challenging to design, as the designer is frequently confronted with contradicting performance requirements, which are calling for various design tradeoffs. Two specifications that are most frequently of highest interest are (i) the mechanical range of motion and (ii) the achievable positioning or scanning speed, which can typically be related to the bandwidth [9]. Besides these two mostly contradicting system requirements, the combination of both properties in terms of the safe operating area is often of even higher practical importance, providing e.g. information on admissible combinations of amplitude and frequency for a certain scan trajectory type. Particularly the product of range times bandwidth appears as additional valuable figure of merit for describing the performance of the scanning unit [10], [11].

When designing a mechatronic positioning or scanning system, there is usually a large number of design parameters that need to be determined and several constraints from different physical domains, e.g. electrical, magnetic or thermal, that need to be considered [2]. Additionally, many of these parameters and design choices are influencing not only a single performance aspect but several system properties, e.g. the sensor bandwidth, which influences the achievable system bandwidth as well as the resulting positioning uncertainty [12]. Various components including sensors (e.g. bandwidth and range), mechanical structure (e.g. structural modes), drivers and the control system as well as their interrelations are important in this relation [13]. As in mechatronic system design actuators are, however, the components in which the major amount of energy is transduced and dissipated and which are predominantly determining the mechanical structure of the system (e.g. the use of a piezo actuator will always result in a high stiffness system), they are considered the dominant and foremost performance determining system component,

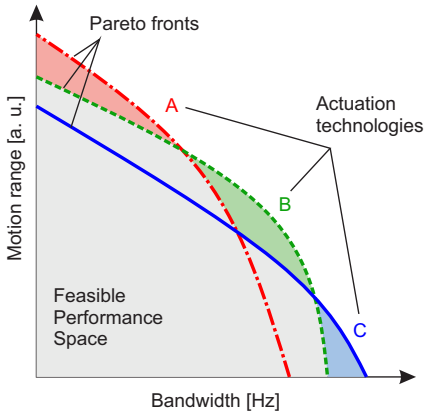

Fig. 1. Schematic of a two-dimensional range-and-bandwidth performance space with Pareto fronts of three different actuation technologies. The Pareto front defines the maximal achievable performance for a tradeoff between range and speed. The colored areas represents requirement combinations for which one technology is superior to all other ones.

The authors are with the Christian Doppler Laboratory for Precision Engineering for Automated In-Line Metrology at the Automation and Control Institute (ACIN), Vienna University of Technology, 1040 Vienna, Austria. Corresponding author: csencsics@acin.tuwien.ac.at.

Post-print version of the article: E. Csencsics and G. Schitter, "Exploring the Pareto Fronts of Actuation Technologies for High Performance Mechatronic Systems," *IEEE Transactions on Mechatronics*, in press, 2020. DOI: 10.1109/TMECH.2020.3016087

when considering the two mentioned specifications of range and speed [14]. Despite their importance, there is sometimes the tendency to chose actuators for a system based on preferences of the designer or historical reasons, such as piezos for AFMs [4] or electromagnetic actuation in wafer scanners [1], rather than on an analytic evaluation and comparison of various applicable technologies, such that more appropriate alternatives enabling higher performance may be overlooked (cf. Fig. 1) [15].

To enable a more systematic and fact-based actuator choice, several approaches have been reported recently, ranging from general purpose classifications and selection methods for a large variety of actuators [9] to automated actuator selection algorithms based on a database with several hundred actuators from 18 actuator classes [16]. However, for the system designer who wants to push the system performance to the physical limits, a procedure more focused on the particular system class and relevant technologies, rather than on a database of various commercially available actuators, clearly excluding custom made solutions, might be of even higher relevance. Such an approach has been investigated for the design of single-phase rectifiers to trade off the contradicting system properties efficiency and power density by employing analytic relations to obtain and compare the Pareto fronts of several rectifier topologies [17], [18]. In this the Pareto front of a topology represents the limit curve for tradeoffs between efficiency and density, i.e. Pareto optimal solutions of the optimization problem, separating feasible from non-feasible combinations in a multi-dimensional performance space. Following this idea the Pareto fronts for several actuation technologies could be obtained for a desired mechatronic system class, as shown in Fig. 1, directly indicating e.g. the maximal achievable bandwidth for a required system range. By comparing the Pareto fronts of admissible actuation technologies a fact-based decision for the most appropriate or superior actuation principle for the desired specification can be enabled.

As a first step towards Pareto optimal mechatronic systems, the contribution of this paper is a method for estimating the Pareto fronts of established actuator technologies for a desired class of mechatronic scanners, which are considered the foremost performance determining system component. For this purpose the Pareto fronts of the range-bandwidth tradeoff are directly estimated from analytically obtained relations for each technology. The method is presented along the example of the system class of fast steering mirrors (FSMs) [13], which is well suited for this approach as several Lorentz force [19], piezoelectric [20] as well as hybrid reluctance [21] actuated commercial and academic systems are reported, which can serve as basis to validate the Pareto front estimates. As illustrated in Fig. 1, this approach enables an immediate identification of the actuation principle best suited for satisfying desired range and bandwidth requirements close to the limits of physics (see colored areas in Fig. 1). The specific properties and application classes of FSMs are presented in Section II, together with a discussion on the safe operating area of these systems. In Section III the proposed method is presented, establishing analytical relations between achievable range and bandwidth for estimating the Pareto front for each of the three actuation technologies. For validating the obtained relations they are combined with real-world system parameters in Section IV and compared to a thorough review of reported FSMs. Section V concludes the paper.

II. Fast Steering Mirrors

Fast steering mirrors (FSMs) are a well established technology for scientific and industrial applications that require steering operations of light beams in two dimensions and demand a fast and compact optical device, providing sufficient angular range as well as high angular resolution and positioning bandwidth [21].

A. System Overview

Besides the actuation system, generating the tip and tilt motion of the mover, FSMs comprise the following key components: the mirror, the suspension, the sensor and the position control system [22]. Fig. 2 shows a schematic exploded view of a FSM with its main components, which are briefly discussed in the following.

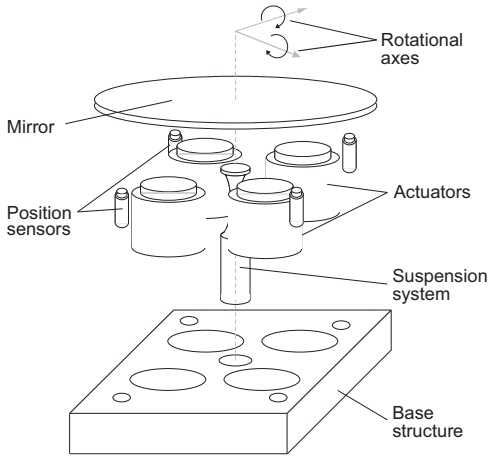

Fig. 2. Fast steering mirror systems for pointing and scanning operations. The exploded view of a basic FSM system structure shows its main components including mirror, actuators, position sensors and suspension system.

The mirror as the optical element reflects and steers an incoming light beam of a defined aperture towards a single specific target position or scans the light beam at a desired speed along a defined trajectory. The critical aspects when designing the mirror are to keep it as light as possible, in order to enable high accelerations of the mover, and to simultaneously make the mirror sufficiently stiff in order to avoid dynamic deformations [19].

The suspension system connects the mirror carrying mover with the static part and is most commonly implemented by a metallic flexure [23]–[25] enabling motion in the actuated rotational degrees of freedom (DoFs) and restricting the non-actuated DoFs. Next to low and high stiffness in the actuated and non-actuated DoFs, respectively, typical requirements include low mechanical hysteresis, stabilization of the pivot

Post-print version of the article: E. Csencsics and G. Schitter, "Exploring the Pareto Fronts of Actuation Technologies for High Performance Mechatronic Systems," *IEEE Transactions on Mechatronics*, in press, 2020. DOI: 10.1109/TMECH.2020.3016087

point, high resistance to fatigue and a thermal expansion coefficient compatible with the mirror [26].

The sensor system is used to measure the tilt angle of the mirror in both axes, for the use in feedback control. Typical non-contacting sensors are based on eddy currents [27], [28], capacity changes [22], [29] or optical principles [30]. Mostly a differential measurement system with two sensors per axis is implemented.

The position control system is necessary to achieve precise motion at high speeds and enable rejection of external disturbances. FSMs are typically operated with high bandwidth feedback controllers to enable fast motion control and disturbance rejection [31], [32]. Frequently used controller types are PID and model-based controllers for low stiffness systems [21] and PI controllers for high stiffness FSM systems [33]. Model-based dual tone feedback controllers with high control gains localized at the drive frequencies of a desired Lissajous trajectory for a defined scan task are also reported [13].

Depending on the application requirements, such as scan range and system bandwidth, electromagnetically [21], [34] and piezoelectrically actuated systems [35], [36] are reported. Independent of the actuator technology the actuators are typically operated in a push-pull configuration with two actuators per axis, in order to generate a pure moment around the center of rotation [35], [37], [38].

B. Application Areas and Performance Requirements

The applications of FSM systems can be separated into two major classes of operation modes: (i) pointing and tracking and (ii) scanning operations [21]. Applications of the first class include tasks like beam stabilization [21], acquisition of optical signals and tracking of objects [39], as well as precise pointing of laser beams [30]. Typical applications from the class of scanning operations are ranging from laser scanners [7] over scanning confocal microscopy [40] to scanning optical lithography [41], optical free space communication [35] and material processing [25].

Pointing and tracking applications comprising an FSM system require good disturbance rejection capabilities as well as high pointing precision, which is typically realized by the integration of high bandwidth position feedback controllers and high resolution position sensors [39]. The typically required motion amplitudes for disturbance rejection decrease quickly for increasing frequency components of the disturbance, such that a low inertia of the FSM mover is not particularly critical [35]. For acquisition of a pointing target the required angular range is typically comparable to the range of scanning systems.

The requirements when operated in scanning mode include high scan speeds (frame rates), large high frequency motion amplitudes and high precision tracking of a reference trajectory. Approaches to reach these requirements for typically demanded compact system dimensions are light weight designs of the mover and high bandwidth feedback control [26] or mechanically tuned system designs for defined trajectory types, such as Lissajous trajectories [13]. The application dependent performance requirements on FSMs are summarized in Table I.

With the competing requirements of speed and range particularly inherent to scanning applications, the evaluation of actuation technologies focuses on this application class.

TABLE I
FSM PERFORMANCE REQUIREMENTS FOR APPLICATION CLASSES.

	Pointing	Scanning
System range	large	large
System dimensions	arbitrary	compact
Main objective	dist. rejection	tracking
Bandwidth	high	high
Motion amplitude	small	large
Mover inertia	arbitrary	small
Precision	high	high

C. Safe Operating Area

The concept of the safe operating area (SOA) is an important performance property from the domain of power electronics [42], which can also be applied to mechatronic scanning systems, for which typically only range and small signal bandwidth are given. It can be used to relate the frequency of mostly a sinusoidal reference trajectory to the maximum admissible scan amplitude that still stays within the operational limits of the system.

Electromagnetically actuated systems are typically limited by the maximum admissible ohmic power loss in the coils and thus by a maximum admissible current density $j_{I,max}$.

The range of piezo actuated systems is determined by the nominal actuator range, which is linked to the blocking force via the actuator stiffness, the stiffness of the pre-tensioning spring, necessary for dynamic operation, and geometric design parameters [2]. Working against a mechanical spring with constant stiffness, piezo actuated systems can thus be typically operated with the maximum scan amplitude up to the system bandwidth, considering power electronics that are capable of driving the capacitive load also at high frequencies.

Figure 3 shows experimentally obtained SOAs with sinusoidal reference signals measured for a custom made piezo actuated (PZA) FSM [43], two commercial Lorentz force actuated (LFA) FSMs with 1 inch and 2 inch mirror (Type: OIM101 and OIM102, Optics in Motion LLC, Long Beach, USA) and two experimental hybrid reluctance actuated (HRA) FSM systems with 1-inch [11] and 2-inch mover [44].

The HRA FSMs have a mechanical system range of $\pm 3°$ and are in terms of the SOA clearly superior to the Lorentz actuated FSMs over the entire frequency range. At the individually specified small signal -3 dB bandwidth all four electromagnetically actuated FSMs are still capable of scanning at an amplitude of about 1% of the system range. The range of the piezo actuated system is with $\pm$ 2.4 mrad significantly smaller than those of the HRA and LFA systems but it enables larger scan amplitudes at frequencies beyond 500 Hz. This observation already provides a first insight into the advantages of the individual actuation technologies and confirms that piezos are typically used for systems with high bandwidth and

Post-print version of the article: E. Csencsics and G. Schitter, "Exploring the Pareto Fronts of Actuation Technologies for High Performance Mechatronic Systems," *IEEE Transactions on Mechatronics*, in press, 2020. DOI: 10.1109/TMECH.2020.3016087

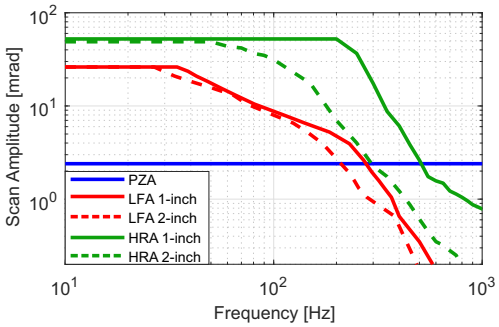

Fig. 3. Measured safe operating area (SOA) of closed-loop FSM systems for sinusoidal reference signals. The SOAs of one piezo actuated (blue), two Lorentz force actuated (red) and two hybrid reluctance actuated FSMs (green) are depicted.

small range, while electromagnetically actuators are employed for systems with large range but smaller bandwidth [26]. However, a characterization of the tradeoff between range and bandwidth and the limitations of each individual technology requires a more formalized approach.

III. Limitations of Actuation Technologies

For investigating the physical limitations of each actuation technology in the context of FSM system design, analytic relations between these two properties are established, with respect to the tradeoff between system range and bandwidth. These relations are then used to estimate the tradeoff limit curves of each actuation technology, i.e. the Pareto front, which is the set of all Pareto-optimal design solutions, separating feasible from non-feasible specification combinations in the performance space [17]. For design solutions along the Pareto front the improvement of e.g. speed results in any case in a reduction of the range and vice-versa.

A. Piezo Actuation

Piezo (PZ) actuated FSMs are in general high stiffness systems, for which the bandwidth limitation for feedback control is typically given by the first mechanical resonance [4]. For actuating the mirror of a FSM in both rotational directions, piezo actuated FSMs are typically equipped with two pairs of stack actuators (see Fig. 4b), aligned along the two system axes and operated in a push-pull configuration. The mover is mostly suspended by a stiff metallic flexure, which connects mover and stator part and provides the pre-stressing of the piezo stacks, required for dynamic operation [43]. Figure 4a shows a cross section schematic of one system axis with the pair of actuators and a generic suspension system. When the mirror is in its neutral position both actuators are extended by half their range, in order to enable bi-directional rotational motion of the mover [4]. With the length of the stack actuator L, a typical stroke of a actuator of around 0.1% of its length, and the distance of the stacks to the center of rotation d (see Fig. 4a) the angular range of the FSM is found by

$$\varphi = \frac{L}{2 \cdot 1000 \cdot d}. \tag{1}$$

Due to the rotational motion of the mover and the required force interface [43], the piezo stacks can be considered held fixed on one end, such that the relation [10]

$$f_{res,PZA} = \frac{1}{2\pi L}\sqrt{\frac{3E}{\rho_{piezo}}} = \frac{1}{2\pi \cdot 2000 \cdot d \cdot \varphi}\sqrt{\frac{3E}{\rho_{piezo}}}, \tag{2}$$

between the first resonance frequency $f_{res,PZA}$ and the actuator length L or the achievable angular range φ can be established, respectively, with E being the elastic modulus and ρ_{piezo} the density of the piezo material. With the first resonance of the actuator determining the maximum achievable bandwidth, this results in an inversely proportional relation $f_{max,PZA} \propto 1/\varphi$, which equals a -1 slope, i. e. -20dB/decade, in a double-logarithmically scaled design space.

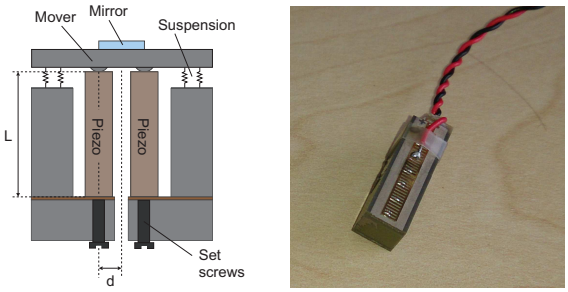

(a) Piezo actuated FSM cross section. (b) Piezo stack.

Fig. 4. Piezo actuation in FSM systems. (a) shows a schematic of the cross section of a piezo actuated FSM system with two actuators operated in push-pull configuration. The springs represent the flexure stiffness. (b) depicts a piezo stack actuator (PICMA stack actuators, Model P-885.91, Physik Instrumente GmbH & Company KG, Germany), typically employed in FSMs.

B. Lorentz Force Actuation

Lorentz force (LF) actuated FSMs, also known as voice coil actuated (VCA) FSMs, are in general low stiffness systems, which typically have a control bandwidth beyond the suspension mode that is usually limited by the internal modes of the moving part [2]. In contrast to the suspension's stiffness dominating the dynamics of high stiffness systems, the mover's mass is dominating the dynamics of low stiffness systems beyond the suspension mode. Via its applied current a given actuator generates a certain force, in dependence on its motor constant, and therewith an acceleration of the mover, which can be increased by applying higher actuator currents. This, however, results in a higher energy dissipation in the coils, which eventually limits the maximum acceleration value. To obtain a figure of merit for the design of efficient LF actuated systems based on this notion, the expression [2]

$$Q = \frac{\alpha}{\sqrt{P}} \tag{3}$$

can be used, giving the angular acceleration α that can be obtained per unit of dissipated power P, which is almost entirely resistive loss, as typical movements are still rather small. The higher the number, the more efficient the actuator is. Using Newton's second law of motion $T = Jalpha$, with

Post-print version of the article: E. Csencsics and G. Schitter, "Exploring the Pareto Fronts of Actuation Technologies for High Performance Mechatronic Systems," *IEEE Transactions on Mechatronics*, in press, 2020. DOI: 10.1109/TMECH.2020.3016087

torque T and mover inertia J, the Lorentz force $F = BIl_{w,a}$, the relation for ohmic power loss $P = I^2R$ in the expression for the figure of merit and considering that the torque in a rotational FSM system is generated by two actuators in push-pull configuration and distance d to the point of rotation, results to

$$Q = \frac{T}{J\sqrt{P}} = \frac{2dF}{J\sqrt{P}} = \frac{2dBIl_{w,a}}{J\sqrt{P}} = \frac{2dBl_{w,a}}{J\sqrt{R}}. \quad (4)$$

In this relation B is the magnetic flux density in the air gap, I is the actuator current and $l_{w,a}$ is the active, force-generating length of the coil wire in the air gap. The total ohmic resistance R of the actuator winding can further be found by

$$R = \frac{\rho_r(l_{w,a} + l_{w,p})}{A_w}, \quad (5)$$

with ρ_r the specific resistance of the wire material, $l_{w,p}$ the length of the non-active coil part, not generating any force (e.g. overhung coil design), and the wire diameter $A_w = \gamma A_c/N$, expressed via coil cross section A_c, fill factor of the coil winding γ and number of turns N [2]. By defining the active coil volume $V_{c,a} = A_c \cdot l_{w,a}$ the actuator design parameter dependent figure of merit can be formulated as

$$Q = \frac{\alpha}{\sqrt{P}} = \frac{2dB}{J}\sqrt{\frac{\gamma V_{c,a}}{n\rho_r}}\sqrt{\frac{l_{w,a}}{l_{w,a} + l_{w,p}}}. \quad (6)$$

The analysis of the SOA of FSM systems in Section II-C showed that the commercial LFA as well as the HRA FSMs are able to perform a sinusoidal scan motion with an amplitude of about 1% of the system range r at a scanning frequency equal to their closed-loop small signal bandwidth. For the further analysis the maximum small signal bandwidth of a low stiffness system is thus considered to be given by the maximum frequency at which the system is still capable of performing a sinusoidal scan with an amplitude of 1% of the system range r. The following derivations are of course also viable for larger amplitudes, e.g. 10% of the system range, and would simply result in an altered (lower) constant k_{LFA} (cf. (10)). Bandwidth-limiting structural modes of the moving part are assumed to occur only at frequencies beyond this small signal bandwidth. The acceleration of the mover for a sinusoidal excitation with small signal amplitude $A_{min} = \varphi/100$ is obtained by the second derivative of the reference signal

$$\ddot{x_r}(t) = \alpha(t) = -(2\pi f)^2 \cdot A_{min} \cdot sin(2\pi f t). \quad (7)$$

Substituting the expression for the acceleration amplitude into the definition of the figure of merit and rearranging the equation in order to obtain the highest attainable small signal frequency, results to

$$f_{max,LFA} = \frac{1}{2\pi} \cdot k_{LFA} \cdot \sqrt{\frac{1}{\varphi \cdot J}}, \quad (8)$$

with the constant k_{LFA} given by

$$k_{LFA} = \sqrt{100 \cdot B \cdot 2d \cdot \sqrt{P \cdot \frac{\gamma V_{c,a}}{N\rho_r} \cdot \frac{l_{w,a}}{l_{w,a} + l_{w,p}}}}. \quad (9)$$

Under the assumption that the maximum value of dissipated power is determined by the maximum current density $j_{I,max}$ and is given by $P_{max} = I_{max}^2 R = j_{I,max}^2 A_w \rho_r l_w$ the factor k_{LFA} results to

$$k_{LFA} = \sqrt{100 \cdot B \cdot 2d \cdot j_{I,max} \cdot \frac{A_c\gamma}{N} \cdot l_{w,a}}. \quad (10)$$

In FSM systems mostly moving magnet designs are employed in order to avoid thermal stress and deformations of the mirror due to losses in the actuator coils [26]. To maintain a low mover inertia the magnet assemblies are kept compact, such that overhung coil designs are commonly used (see Fig. 5c). Figure 5 shows common implementations of LF actuators with overhung coil and overhung magnet designs. Highly efficient LF actuators with a large Q value for an FSM

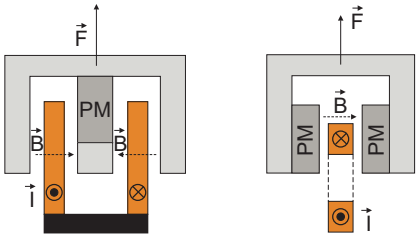

(a) Classic voice coil actuator (b) Overhung magnet design.
in overhung coil design.

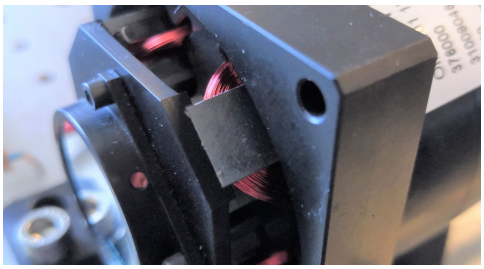

(c) Overhung coil design of OIM FSM.

Fig. 5. Lorentz force actuator designs [2]. (a) shows the cross section of a voice coil design with overhung coil. (b) depicts a schematic of an overhung permanent magnet design and (c) the implementation of an overhung coil design in a commercial FSM.

with a desired range of angular motion will aim to minimize mover weight and coil length to enable the desired range. An increase in angular range of the FSM will thus entail an increased length and weight of the actuator's moving part as well as a larger inertia of the entire FSM mover. With the initial inertia of the mover J_{init} and the inertia increase per range Δ_J, the range r dependent total inertia is found by

$$J = J_{init} + \Delta_J \cdot r. \quad (11)$$

This assumption is applicable to most relevant practical actuator solutions, targeting a high figure of merit, independent of a moving coil/magnet configuration or an overhung coil/magnet design.

Using (11) and the small angle approximation $r = 2\varphi d$ in (8) results in the final formulation of the relation between

Post-print version of the article: E. Csencsics and G. Schitter, "Exploring the Pareto Fronts of Actuation Technologies for High Performance Mechatronic Systems," *IEEE Transactions on Mechatronics*, in press, 2020. DOI: 10.1109/TMECH.2020.3016087

range and small signal bandwidth for LF actuated FSMs

$$f_{max,LFA} = \frac{1}{2\pi} \cdot k_{LFA} \cdot \sqrt{\frac{1}{(\varphi J_{init} + \Delta_J \cdot 2d\varphi^2)}}. \quad (12)$$

For small angular ranges φ the first term in the denominator dominates, which makes $f_{max,LFA} \propto 1/\sqrt{\varphi}$ and results in a -2 slope, i. e. -40 dB/decade, in the double-logarithmically scaled design space. At large angular ranges φ the second term dominates, such that $f_{max,LFA} \propto 1/\varphi$, which again equals a -1 slope in a double-logarithmic representation of the design space. The required coil clearance of the actuators also needs to be considered in the design of large range systems and might require custom made solutions to maintain short air gaps in the magnetic circuit [26].

C. Hybrid Reluctance Force Actuation

Hybrid reluctance (HR) actuators provide higher motor constants than LF actuators [45], thus enabling FSM systems with larger SOA, as shown in Fig. 3. As in the case of the LF actuated FSMs, HR actuated FSMs typically have control bandwidths beyond the suspension mode [44]. Figure 6 shows two implementations of HR actuators for FSM systems and illustrates their working principle [21], [44]. The magnetic bias flux (red) generated by the permanent magnet in the center passes through the ferromagnetic mover and the working air gaps and returns via the outer ferromagnetic yoke parts. The permanent magnet introduces a negative stiffness and leads to an inherently open-loop unstable system, which is usually made open-loop stable by a metallic flexure suspending the mover. The coils are connected in series such that an applied current generates a magnetic flux (blue) passing through the outer yoke parts, the working air gaps and the mover. A superposition of both magnetic fluxes results in an increased magnetic flux in one and a reduced magnetic flux in the other working air gap, generating a translational force on the mover in Fig. 6a and a torque on the mover in Fig. 6b, dependent on the coil current direction. For generating tip and tilt motion in FSM systems, four of the actuators in Fig. 6a are place around the mirror, with the mover of the actuator connected to the mirror [21]. Combining the actuator in Fig. 6b in a perpendicular configuration with a second of its kind, enables torque generation around both axes while placing all components behind the mirror plane [11].

The limitations on the achievable closed-loop bandwidth result again from either (i) structural modes of the system or (ii) the maximum coil current density, which is applicable to stay within the thermal limits of the actuator. Eddy currents in the ferromagnetic yoke parts can cause additional phase lag in the system limiting the bandwidth [46], which may, however, be compensated by replacing an underlying current feedback loop by flux feedback control [47]. In any case the phase loss due to eddy currents depends solely on the conductivity and permeability of the yoke material as well as on the layer thickness in systems with layered yoke parts [48], such that there is no relation to air gap length and range.

In contrast to LF actuated systems the mover mass m (translation) or inertia J (rotation) is independent of the system

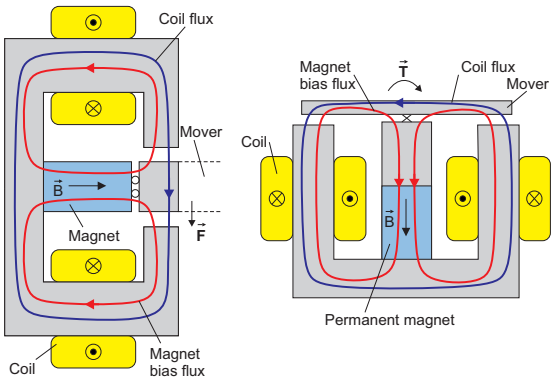

(a) HRA for translational motion.

(b) HRA for rotational motion.

Fig. 6. Hybrid reluctance actuator designs. (a) shows a translational HRA, which is arranged on both sides of a mover to generate the required torque around the center of rotation [2]. (b) depicts a modified HRA for rotational motion [44].

range in the case of an HR actuator, as no actuator parts need to be attached to the mover (see Fig. 6). However, an increased motion range requires increased air gap lengths reducing the maximum applicable actuator torque, which can for the actuator in Fig. 6b be approximated by [44]

$$T_{max} \approx \underbrace{N i_{max} \cdot \frac{l_m}{l_m + l_n} \cdot d \cdot \frac{\mu_0 H_c A_p}{4}}_{X_{T_0}} \cdot \frac{1}{(l_{w0} + l_x)}, \quad (13)$$

with N the number of coil windings, H_c the coercivity and l_m the length of the permanent magnet, l_n the length of the non-working air gap, μ_0 the permeability of vacuum, d the lever arm, A_p the cross section, and l_{w0} the length of the working air gaps in the middle position. The maximum torque is eventually bounded by the saturation flux density of the yoke and mover material, beyond which the ferromagnetic parts saturate and no additional torque increase can be obtained. This saturation effect can be considered by a minimum length of the working air gap l_x.

Making the same assumptions for the relation between small signal amplitude (again 1% of the system range) and achievable system bandwidth as for the LF actuated systems, gives the relation

$$T_{max} = J \cdot \alpha_{max} = J \cdot (2\pi f_{max})^2 \cdot \frac{\varphi}{100}. \quad (14)$$

Combining (13) and (14), using the small signal approximation $l = \varphi d$ for l_{w0} and l_x and rearranging the equation to obtain the highest attainable small signal frequency, results to

$$f_{max,HRA} = \frac{1}{2\pi} \cdot k_{HRA} \cdot \sqrt{\frac{1}{\varphi_x \varphi + \varphi^2}}, \quad (15)$$

with the constant k_{HRA} given by

$$k_{HRA} = \sqrt{\frac{100 \cdot X_{T_0}}{dJ}}. \quad (16)$$

For large angular ranges φ the denominator of (15) is

Post-print version of the article: E. Csencsics and G. Schitter, "Exploring the Pareto Fronts of Actuation Technologies for High Performance Mechatronic Systems," *IEEE Transactions on Mechatronics*, in press, 2020. DOI: 10.1109/TMECH.2020.3016087

dominated by the second term, such that $f_{max,HRA} \propto 1/\varphi$, resulting in a -1 slope in the double-logarithmically scaled design space. Towards angles increasingly smaller than φ_x the first term starts to dominate, making $f_{max,HRA} \propto 1/\sqrt{\varphi}$ and resulting in a -2 slope in the design space.

IV. Pareto Front Estimates for FSM Systems

In order to get an overview of the limitations of real world FSM systems as basis for obtaining a Pareto front estimate (PFE) for each actuation technology, a thorough literature research on reported commercial as well as academic FSM systems is conducted. The evaluated systems are entered into a double logarithmically scaled 2-dimensional performance space with small-signal bandwidth and angular range on the x- and y-axis, respectively, which is depicted in Fig. 7. FSM systems located farther up-right show a larger product of range times bandwidth (RBP), which serves as performance metric for the comparison of system performance in the following and is basically a first order approximation of the SOA introduced in Section II-C. In Fig. 7 lines of constant RBP are shown for the - in this sense - best performing FSM system of each actuation technology. The highest RBP values obtained for PZA, LFA and HRA FSMs are 16320 mrad·Hz [33], 61100 mrad·Hz [19] and 78600 mrad·Hz [11], respectively.

In the following a PF for each actuation technology is estimated by evaluating the equations derived in the previous section for the parameters of the respectively best performing FSM system. These systems are considered to be ones closest to the true Pareto front of each technology, thus enabling a reasonable determination of the related PFE. It is to be considered at this point that the resulting PFEs are based on current state of the art FSM systems and their system parameters, which means that the state of the art in FSM system design suggests that these are the current Pareto fronts. Prospective improvements and innovations of materials (e.g. piezo material), motor constants, power electronics and other aspects may, however, enable to shift the Pareto fronts to even higher performance levels in the future.

A. Piezo Actuation

The relation between resonance frequency $f_{res,PZA}$ and angular range φ for a piezo actuated FSMs with stacks held fixed on one end is given in Eq. (2). To account for the mass of the mover m_{end} which is added to the free end of the actuator stacks, this relation is extended by an additional denominator term which refers to the related reduction of the resonance frequency [10]. The resulting expression is

$$f_{res,PZA} = \frac{1}{2\pi}\sqrt{\frac{AE}{\frac{1}{3}A(2000d)^2\rho_{piezo}\cdot\varphi^2 + m_{end}2000d\cdot\varphi}}. \quad (17)$$

with A the cross section area of the stacks and the other parameters as given in Section III-A. For values of $\varphi >> 3m_{end}/2000Ad\rho_{piezo}$ the second denominator term can be neglected and the initial relation from Eq. (2) is obtained, resulting in a -1 slope in the design space. For small values of φ the second denominator term starts to dominated, resulting in a -2 slope at higher frequencies.

From the graph in Fig. 7 it can be seen that the piezo FSM with ± 2.4 mrad angular range and a resonance frequency of 6.8 kHz results to the highest RBP value of 16320 mrad·Hz [33]. The system is depicted in Fig. 8a, uses 4 of the piezo stacks shown in Fig. 4 (Model P-885.91, Physik Instrumente GmbH & Company KG, Germany) for actuation and uses a membrane-like flexure to maximize the system's RBP. With the FSM system parameters m_{end} = 5 g (half mover mass), A = 5 x 5 mm^2 and d = 6 mm and typical parameters of piezo stack actuators E = 33.9 GPa and ρ_{piezo} = 8000 kg/m^3 [10], the PFE shown in Fig. 7 (dash-dotted, blue line) can be obtained. In the area where the PFE is backed by the specifications of real world systems the PFE is depicted as bold dark blue line, while the estimate is shown as a thinner light blue line towards larger ranges and bandwidths. The used piezo system lies slightly below the resulting PFE, which has a -1 slope at low frequencies and changes to a steeper -2 slop at around 8 kHz, indicating that there is still room for performance improvement.

B. Lorentz Actuation

For obtaining the PFE for LF actuated FSMs Eq. (10) and Eq. (12) can directly be used. As there was not sufficiently detailed data for the academic FSM system with the highest RBP [19] available, the properties of a high end commercial FSM (OIM101 FSM, Optics in Motion LLC, Long Beach, USA), which has an RBP value of 22270 mrad·Hz and is marked by the thick red diamond in Fig. 7, are used to obtain the shape of the PFE. The measured complementary sensitivity function of the LFA FSM system (see Fig. 5) with a feedback controller tuned for maximum bandwidth measured and small signal excitation is depicted in Fig. 8c.

The mechanical parameters for the inertia and the range dependent inertia increase are obtained from the CAD file of the mirror system provided by the manufacturer and result to J_{init} = 3925 g·mm^2 and Δ_J = 350 g·mm^2/mm. The lever arm of the actuators is d = 15 mm. The actuator parameters are determined by examining the data sheet and the system in the laboratory, resulting to a maximum admissible current of I_{max} = 1.622 A per axis, obtained from the peak power given in the data sheet and the measured resistance of one coil pair of R = 5.7 Ω, N = 140 coil turns and $l_{w,a}$ = 1300 mm, due to a magnet width of about 10 mm and the overhung coil design (see Fig. 5c). The flux density in the air gap is measured by a Gauss-Meter and results B = 0.6 T. Considering that the maximum admissible current can be expressed by $I_{max} = j_{I,max}\cdot A_c\gamma/N$, this yields in total a factor of k_{LFA} = 1.948 kg$^{0.5}$m/s, according to Eq. (10). The resulting graph, depicted in Fig. 7 (dashed red line), lies just beyond the commercial FSM (thick red diamond), demonstrating the validity of the obtained relation between range and bandwidth. It shows a -2 characteristic for angles smaller than ± 300 mrad to a -1 characteristic for larger angles.

To extrapolate the obtained graph in order to arrive at a PFE for LF actuated FSMs, which estimation should be based

Post-print version of the article: E. Csencsics and G. Schitter, "Exploring the Pareto Fronts of Actuation Technologies for High Performance Mechatronic Systems," *IEEE Transactions on Mechatronics*, in press, 2020. DOI: 10.1109/TMECH.2020.3016087

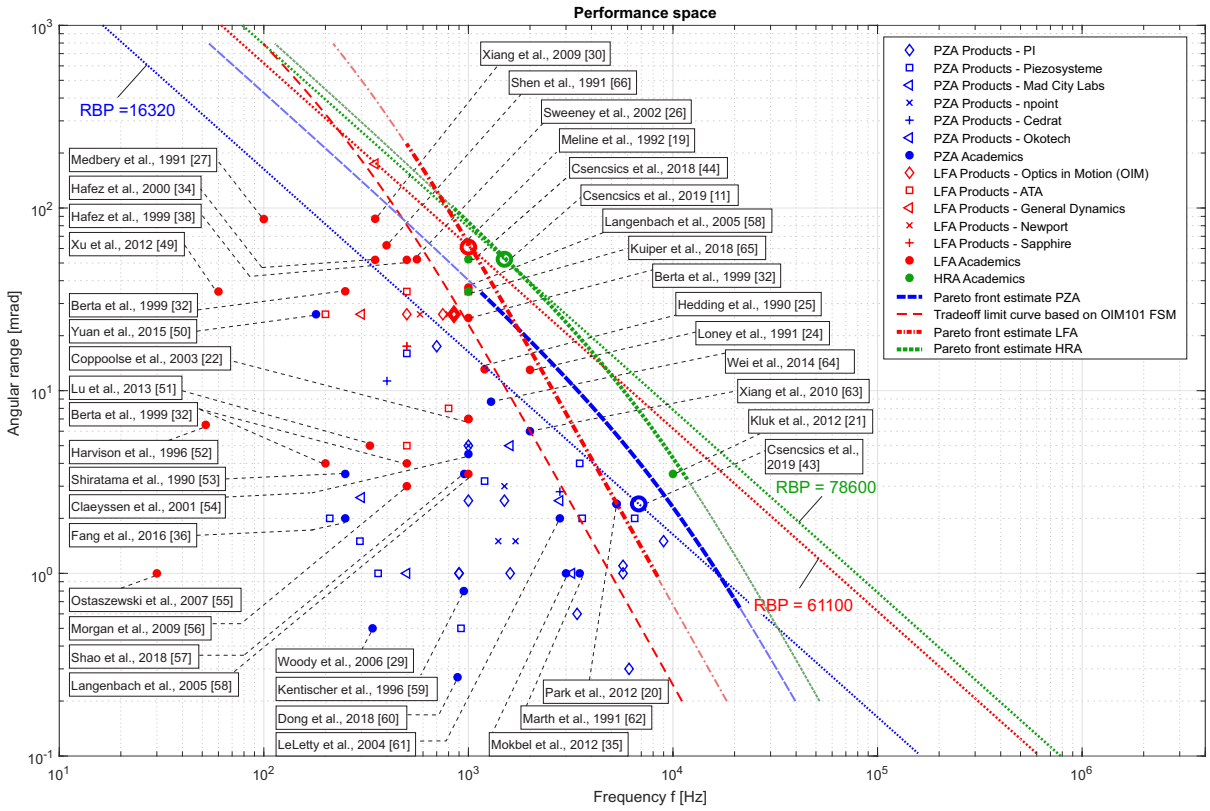

Fig. 7. Two dimensional performance space for FSM systems showing the tradeoff between range and bandwidth. Commercially available (symbols) as well as academically reported systems (dots) actuated by piezo (blue), Lorentz force (red) and reluctance actuators (green) are depicted. The Pareto front estimate for each actuation technology is derived from the calculated relations between frequency and range. Additionally lines of constant range-bandwidth-product are depicted for the best performing system, with the respectively highest value, of each technology.

on the system with the highest RBP value of 61100 mrad·Hz (large red circle), the ratio of the RBP values of both systems p = 61100 / 22270 = 2.74 is used. For the case of angles larger than ± 300 mrad, where the first denominator term of (12) can be neglected and a relation $f_{max,LFA} = c/\varphi$ (c = const.) can be obtained, the ratio p can be directly used to extrapolate the curve via $f_{max,LFA} = c \cdot p/\varphi$. By considering the scaled version $\varphi' = \varphi/p$ as the new angle and using it in (12), the entire extrapolated PFE can be obtained. The extrapolated PFE lies just beyond the best performing LFA FSM and is also depicted in Fig. 7 (dash-dotted red line). It shows the same -2 and -1 characteristic for small and large angles, respectively, with a higher corner frequency. As for the piezo actuated systems the PFE is shown by a bold red line in the area where it is backed by real world system specifications and by a thinner light red line towards higher bandwidths and ranges.

C. Hybrid Reluctance Actuation

For the HRA systems a compact academic FSM with an RBP value of 78600 mrad·Hz [11] is evaluated for its system properties (see Fig. 7). The FSM, which is depicted in Fig. 8b, uses the HR actuator structure shown in Fig. 6 and employs a yoke material with high saturation flux density as well as a flexure-based suspension system. The measured complementary sensitivity function of the HRA FSM system with a feedback controller tuned for maximum bandwidth and small signal excitation is depicted in Fig. 8c.

The maximum torque level is obtained from simulations conducted with ANSYS (Ansys Electronics Desktop, Ansys Inc., PA, USA) and resulting in a torque around the center position of T_0 = 13.3 mNm at the maximum current for continuous operation. The geometrical properties are derived from CAD design files, providing d = 10 mm for the lever arm and about J = 300 g·mm^2 for the mover inertia. With the length of the working air gap in the middle position l_{w0} = 0.75 mm, the constant $X_{T_0} = T_0 \cdot l_{w0}$ is obtained. The minimum length of the working air gap before saturation of the yoke material is obtained by employing electromagnetic simulations in ANSYS Maxwell (Ansys Electronics Desktop, Ansys Inc., PA, USA) and results to l_x = 0.15 mm. This yields a graph with a -1 slope for angles larger than 15 mrad and changes to a steeper -2 slope, which is caused by increasing saturation effects in the ferromagnetic yoke parts. The resulting PFE lies slightly

Post-print version of the article: E. Csencsics and G. Schitter, "Exploring the Pareto Fronts of Actuation Technologies for High Performance Mechatronic Systems," *IEEE Transactions on Mechatronics*, in press, 2020. DOI: 10.1109/TMECH.2020.3016087

beyond the HRA FSM with the highest RBP value, almost intersecting with its location in the design space. As pointed out previously, additional bandwidth limiting dynamics caused by eddy current effects in the yoke parts are not considered in this study. If not compensated by constructional of control means, they may cause an increasing steepness of the graph towards higher frequencies.

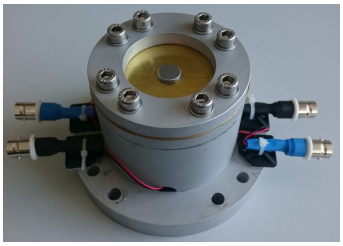

(a) Piezo actuated FSM [43].

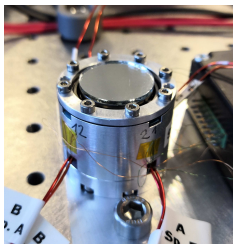

(b) HR actuated FSM [11].

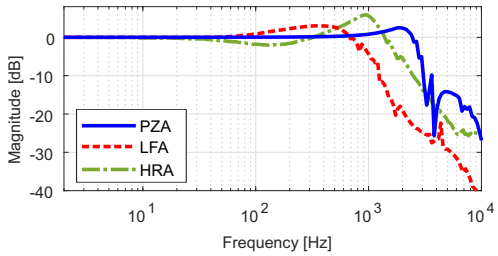

(c) Measured complementary sensitivity functions.

Fig. 8. Experimental high performance FSM systems. (a) shows a piezo actuated FSM with a 1 mm mirror and a flexure optimized for maximum RBP. (b) shows a compact HR actuated FSM system with an range of $\pm$ 3 deg, a bandwidth of 1.5 kHz and an outer diameter as small as 32 mm. (c) depicts the measured small-signal complementary sensitivity functions of the above shown feedback controlled PZA and HRA FSM as well as of the LFA FSM from Fig. 5c with maximized bandwidth.

D. Discussion

The 2-dimensional performance space shown in Fig. 7 with the evaluated FSM systems and the obtained Pareto front estimates clearly illustrates the advantages and limitations of the three established actuation principles and reveals regions in which a particular actuation principle clearly outperforms the other ones. The piezo actuated FSMs have smaller ranges than LFA and HRA systems, but they outperform the LFA FSMs, with the fastest system having at bandwidth of 2 kHz, for system bandwidths above 2 kHz and angular ranges below 20 mrad. The FSMs actuated by LF actuators provide larger angular range as compared to the piezo actuated systems, which have a maximum range of 26.2 mrad, but enable at the same time smaller bandwidths. This makes the LF actuation technology superior over piezo actuation for large stroke systems in the low frequency region. When compared to the more established LF and piezo actuation technologies, the HR actuation technology shows significant advantages over most of the relevant specification range. Despite the small number of reported FSMs using this technology, these systems together with the related PFE suggest that HR actuation is superior to both of the other technologies for FSMs with a bandwidth above 700 Hz and angular ranges below 120 mrad. Due to the enlarged air gaps and the thus decreasing motor constant of the HR actuators, LF actuation is superior for ranges above 120 mrad. Potential additional limitations due to parasitic or nonlinear effects in the ferromagnetic yoke material, such as eddy currents and material hysteresis, might cause a steeper slope of the HRA PFE at higher frequencies, such that piezo actuation may become the superior technology towards higher frequencies.

In summary it is shown that based on the presented analytic approach Pareto fronts can be estimated for various actuation principles of a certain mechatronic system class, which can enable an immediate fact-based identification of the actuation principle best suited for satisfying a given combination of range and bandwidth requirements in the design process.

V. Conclusion and Outlook

This paper presents a novel method for estimating the limitations of individual actuation technologies for mechatronic scanning systems based on analytically obtained relations along the example of fast steering mirrors. It is used to estimate the Pareto fronts for the established piezoelectric, Lorentz force and hybrid reluctance actuation principles in the 2-dimensional range-bandwidth performance space. The obtained equations, relating maximum range and achievable bandwidth, are validated using real world FSM systems in order to get estimates for the individual Pareto front of each technology. These estimates are validated by comparing them to a thorough study on specifications of available commercial and academic FSM systems, showing good agreement with the obtained results in the 2-dimensional performance space. The analysis reveals that the hybrid reluctance technology is superior to the established Lorentz force and piezo actuation technologies for systems with bandwidths above 700 Hz and angular ranges below 120 mrad, enabling the best compromise between range and bandwidth over a large part of the performance space and resulting in the FSMs with the highest RBP value reported so far. The obtained actuator performance map provides a solid basis for the design of future FSM systems, aiming to push their performance towards the limits of physics, and simplifies the selection of the most suitable actuator based on desired system performance requirements.

A generalization of the results obtained for FSMs is desirable but difficult, due to the manifold of design choices and customized solutions among the various mechatronic system classes. However, as the proposed method relies on physical models and analytic equations of the respective system class, which can be individually adapted to their specific properties and requirements, the presented method for obtaining Pareto front estimates appears to be adaptable for and applicable to other mechatronic system classes of comparable complexity. It may be employed during the design process to systematically trade off desired range and speed specifications and enable a fact-based choice of the best-suited actuation technology. The approach may also be advanced to additionally consider e.g. the properties of the power electronics, adapted to to

Post-print version of the article: E. Csencsics and G. Schitter, "Exploring the Pareto Fronts of Actuation Technologies for High Performance Mechatronic Systems," *IEEE Transactions on Mechatronics*, in press, 2020. DOI: 10.1109/TMECH.2020.3016087

trade off other target specifications, such as resolution and bandwidth, or extended to more target specifications and multi-dimensional performance spaces.

An extension of the proposed approach from mechatronic systems on the component level, e.g scanning units, to mechatronic systems on the scale of entire production systems, e.g. lithography machines, may also be desirable and possible in the future.

Acknowledgment

The financial support by the Christian Doppler Research Association, the Austrian Federal Ministry for Digital and Economic Affairs, and the National Foundation for Research, Technology and Development, as well as MICRO-EPSILON MESSTECHNIK GmbH & Co. KG and ATENSOR Engineering and Technology Systems GmbH is gratefully acknowledged.

References

[1] H. Butler, "Position control in lithographic equipment," *IEEE Control Systems Magazine*, vol. 31, no. 5, 2011.
[2] R. M. Schmidt, G. Schitter, A. Rankers, and J. van Eijk, *The Design of High Performance Mechatronics*, 2nd ed. Delft University Press, 2014.
[3] P. Hansma, G. Schitter, G. Fantner, and C. Prater, "High speed atomic force microscopy," *Science*, vol. 314, pp. 601–602, 2006.
[4] G. Schitter, K. J. Astrom, B. E. DeMartini, P. J. Thurner, K. L. Turner, and P. K. Hansma, "Design and modeling of a high-speed afm-scanner," *IEEE Transactions on Control Systems Technology*, vol. 15, no. 5, pp. 906–915, 2007.
[5] M. G. L. Gustafsson, "Surpassing the lateral resolution limit by a factor of two using structured illumination microscopy," *Journal of Microscopy*, vol. 198, no. 2, pp. 82–87, 2000.
[6] H. Yoo, M. Verhaegen, and G. Schitter, "Iterative learning control of a galvanometer scanner for fast and accurate scanning laser microscopy," in *13th Mechatronics Forum International Conference*, Linz, Austria, 2012, pp. 537–543.
[7] J. Schlarp, E. Csencsics, and G. Schitter, "Optical scanning of laser line sensors for 3d imaging," *Applied Optics*, vol. 57, no. 18, pp. 5242–5248, 2018.
[8] S. Ito, M. Poik, E. Csencsics, J. Schlarp, and G. Schitter, "Scanning chromatic confocal sensor for fast 3d surface characterization," *Proceedings of the 2018 Summer Topical Meeting, Advancing Precision in Additive Manufacturing*, no. 226-231, 2018.
[9] A. D. Poole and J. D. Booker, "Design methodology and case studies in actuator selection," *Mechanism and Machine Theory*, vol. 46, no. 5, pp. 647–661, 2011.
[10] Y. K. Yong, S. O. R. Moheimani, B. J. Kenton, and K. K. Leang, "High-speed flexure-guided nanopositioning: Mechanical design and control issues," *Review of Scientific Instruments*, vol. 83, no. 12, p. 121101, 2012.
[11] E. Csencsics, J. Schlarp, T. Schopf, and G. Schitter, "Compact high performance hybrid reluctance actuated fast steering mirror system," *Mechatronics*, vol. 62, p. 102251, 2019.
[12] L. Jabben, D. Trumper, and J. van Eijk, "Dynamic error budgeting-an integral system design approach for high precision machines," *Proc. of EUSPEN*, pp. 363–367, 2008.
[13] E. Csencsics and G. Schitter, "System design and control of a resonant fast steering mirror for lissajous-based scanning," *IEEE/ASME Transactions on Mechatronics*, vol. 22, no. 5, pp. 1963–1972, 2017.
[14] S. Ito and G. Schitter, "Comparison and classification of high-precision actuators based on stiffness influencing vibration isolation," *IEEE Transactions on Mechatronics*, vol. 21, no. 2, p. 1169, 2016.
[15] J. Cuttino, D. Newman, J. Gershenson, and D. Schinstock, "A structured method for the classification and selection of actuators for space deployment mechanisms," *Journal of Engineering Design*, vol. 11, no. 1, pp. 31–53, 2000.
[16] M. Zupan, M. Ashby, and N. Fleck, "Actuator classification and selection - the development of a database," *Advanced Engineering Materials*, vol. 4, no. 12, pp. 933–940, 2002.
[17] J. W. Kolar, J. Biela, and J. Minibock, "Exploring the pareto front of multi-objective single-phase pfc rectifier design optimization - 99.2% efficiency vs. 7kw/dm^3 power density," *IEEE 6th International Power Electronics and Motion Control Conference*, pp. 1–21, 2009.
[18] J. Biela and J. W. Kolar, "Pareto-optimal design and performance mapping of telecom rectifier concepts," *Proc. of the Power Conversion and Intelligent Motion Conference, Shanghai, China*, 2010.
[19] M. E. Meline, J. P. Harrell, and K. A. Lohnes, "Universal beam steering mirror design using the cross blade flexure," *SPIE Vol. 1697 Acquisitino, Tracking and Pointing VI*, pp. 424–442, 1992.
[20] J.-H. Park, H.-S. Lee, J.-H. Lee, S.-N. Yun, Y.-B. Ham, and D.-W. Yun, "Design of a piezoelectric-driven tilt mirror for a fast laser scanner," *Japanese Journal of Applied Physics*, vol. 51, no. 9S2, p. 09MD14, 2012.
[21] D. J. Kluk, M. T. Boulet, and D. L. Trumper, "A high-bandwidth, high-precision, two-axis steering mirror with moving iron actuator," *Mechatronics*, vol. 22, no. 3, pp. 257–270, 2012.
[22] W. Coppoolse, M. Kreienbuehl, J.Moerschell, A. Dommann, and D. Bertsch, "Dual-axis single-mirror mechanism for beam steering and stabilisation in optical inter sattelite links," *10th European Space Mechanisms and Tribology Symposium*, vol. 524, no. 183-190, 2003.
[23] L. Germann and J. Braccio, "Fine-steering mirror technology supports 10 nanoradian systems," *Optical Engineering*, vol. 29, no. 11, pp. 1351–1359, November 1990.
[24] G. C. Loney, "Design of a high-bandwidth steering mirror for space-based optical communications," *SPIE Vol. 1543 Active and Adaptive Optical Components*, pp. 225–235, 1991.
[25] L. R. Hedding and R. A. Lewis, "Fast steering mirror design and performance for stabilization and single axis scanning," *SPIE 340 Vol. 1304 Acquisition, Tracking and Pointing IV*, pp. 14–24, 1990.
[26] M. Sweeney, G. Rynkowski, M. Ketabchi, and R. Crowley, "Design considerations for fast steering mirrors (fsms)," *Optical Scanning 2002, Proceedings of SPIE*, vol. 4773, 2002.
[27] J. D. Medbery and L. M. Germann, "The 6 degree-of-freedom (dof) magnetically-suspended fine-steering mirror," *SPIE Vol. 1482 Acqisition, Tracking and Pointing V*, pp. 397–405, 1991.
[28] P. Bandera, "A fine pointing mechanism for intersatellite laser communication," *EUROPEAN SPACE AGENCY-PUBLICATIONS-ESA SP*, vol. 438, pp. 61–66, 1999.
[29] S. Woody and S. Smith, "Design and performance of a dual drive system for tip-tilt angular control of a 300mm diameter mirror," *Mechatronics*, vol. 16, no. 7, pp. 389–397, Sep 2006.
[30] S. Xiang, P. Wang, S. Chen, X. Wu, D. Xiao, and X. Zheng, "The research of a novel single mirror 2d laser scanner," *Proc. of SPIE*, vol. 7382, Aug 2009.
[31] Y. Xia, Q. Bao, and Q. Wu, "Internal model control of a fast steering mirror for electro-optical fine tracking," *Proc. of SPIE*, vol. 7843, 2010.
[32] A. Berta, L. Hedding, C. Hoffman, and M. Messaros, "Development of a commercial line of high-performance, fast-steering mirrors," *SPIE*, vol. 3787, pp. 181–192, July 1999.
[33] E. Csencsics, B. Sitz, and G. Schitter, "Piezo actuated fast steering mirror system for high speed optical scanning," *8th IFAC Symposium on Mechatronic Systems, Vienna, Austria*, 2019.
[34] M. Hafez, T. Sidler, R. Salathe, G. Jansen, and J. Compter, "Design and simulations and experimental and investigations of a compact single mirror tip/tilt laser scanner," *Mechatronics*, vol. 10, pp. 741–760, 2000.
[35] H. F. Mokbel, W. Yuan, L. Q. Ying, C. G. Hua, and A. A. Roshdy, "Research on the mechanical design of two-axis fast steering mirror for optical beam guidance," *Proceedings of 2012 International Conference on Mechanical Engineering and Material Science (MEMS 2012)*, 2012.
[36] C. Fang, J. Guo, G. Q. Yang, Z. H. Jiang, X. H. Xu, and T. F. Wang, "Design and performance test of a two-axis fast steering mirror driven by piezoelectric actuators," *Optoelectronics Letters*, vol. 12, no. 5, p. 333, 2016.
[37] H. DeWeerd, "Compact, low power precision beam steering mirror," *SPIE Vol. 1454 Beam Deflection and scanning technologies*, pp. 207–214, 1991.
[38] M. Hafez and T. C. Sidler, "Fast steering two-axis tilt mirror for laser pointing and scanning," *SPIE Vol. 3834*, September 1999.
[39] M. Guelman, A. Kogan, A. Livne, M. Orenstein, and H. Michalik, "Acquisition and pointing control for inter-satellite laser communications," *IEEE Transactions on Aerospace and Electronic Systems*, vol. 40, no. 4, p. 1239, 2004.
[40] H. Yoo, M. E. van Royen, W. A. van Cappellen, A. B. Houtsmuller, M. Verhaegen, and G. Schitter, "Automated spherical aberration correction in scanning confocal microscopy," *Review of Scientific Instruments*, vol. 85, p. 123706, 2014.

Post-print version of the article: E. Csencsics and G. Schitter, "Exploring the Pareto Fronts of Actuation Technologies for High Performance Mechatronic Systems," *IEEE Transactions on Mechatronics*, in press, 2020. DOI: 10.1109/TMECH.2020.3016087

[41] Q. Zhou, P. Ben-Tzvi, D. Fan, and A. A. Goldenberg, "Design of fast steering mirror and systems for precision and laser beams and steering," *IEEE International Workshop on Robotic and Sensors Environments, Ottawa, CAN*, 2008.
[42] P. Moens and G. van den Bosch, "Characterization of total safe operating area of lateral dmos transistors," *IEEE transactions on device and materials reliability*, vol. 6, no. 3, pp. 349–357, 2006.
[43] E. Csencsics, B. Sitz, and G. Schitter, "Integration of control design and system operation of a high performance piezo-actuated fast steering mirror," *IEEE Transactions on Mechatronics*, vol. 25, no. 1, pp. 239–247, 2020.
[44] E. Csencsics, J. Schlarp, and G. Schitter, "High-performance hybrid-reluctance-force-based tip/tilt system: Design, control, and evaluation," *IEEE Transactions on Mechatronics*, vol. 23, no. 5, pp. 2494–2502, 2018.
[45] N. H. Vrijsen, J. W. Jansen, and E. A. Lomonova, "Comparison of linear voice coil and reluctance actuators for high-precision applications," *Power Electronics and Motion Control Conference*, 2010.
[46] E. Csencsics and G. Schitter, "Design of a phase-locked-loop-based control scheme for lissajous-trajectory scanning of fast steering mirrors," *2017 American Control Conference, Seattle, WA, USA*, 2017.
[47] F. Cigarini, S. Ito, J. Konig, and G. Schitter, "Compensation of hysteresis in hybrid reluctance actuator for high-precision motion," *8th IFAC Symposium on Mechatronic Systems*, accepted, 2019.
[48] E. Csencsics, J. Schlarp, and G. Schitter, "Bandwidth extension of hybrid-reluctance-force-based tip/tilt system by reduction of eddy currents," *IEEE International Conference on Advanced Intelligent Mechatronics, Munich, Germany*, 2017.
[49] X. Xu, B. Wang, and X. Han, "Fast-steering mirror with self-aligning ball bearing supporting structure," *Proc. of SPIE*, vol. 84180I-84180I, pp. 1–8, Oct 2012.
[50] G. Yuan, D. Wang, and S. Li, "Single piezoelectric ceramic stack actuator based fast steering mirrorwith fixed rotation axis and large excursion angle," *Sensors and Actuators A: Physical*, vol. 235, pp. 292–299, 2015.
[51] Y. Lu, D. Fan, and Z. Zhang, "Theoretical and experimental determination of bandwidth for a two-axis fast steering mirror," *Optik - International Journal for Light and Electron Optics*, vol. 124, no. 16, pp. 2443–2449, 2013.
[52] D. A. Harvison and B. Hardy, "Precision pointing mechanism for laser communication mission," *SPIE*, vol. 2807, pp. 142–147, 1996.
[53] K. Shiratama, T. Hamuro, Y.Ohgushi, and M. Shimizu, "Fine pointing mechanism using multi-layered piezo-electric actuator for optical isl system," *SPIE Vol. 1218 Free-Space Laser Communication Technologies II*, pp. 117–128, 1990.
[54] F. Claeyssen, R. L. Letty, F. Barillot, N. Lhermet, H. Fabbro, P. Guy, M. Yorck, and P. Bouchilloux, "Mechanisms based on piezo actuators," *Smart Structures and Materials 2001: Industrial and Commercial Applications of Smart Structures Technologies*, vol. 1218, pp. 225–234, 2001.
[55] M. Ostaszewski and W. Vermeer, "Fine steering mirror for the james webb space telescope," *Proc. of SPIE*, vol. 6665-66650D, pp. 1–10, 2007.
[56] F. Morgan, S. Wasson, J. London, J. Kern, M. Smith, R. Sullivan, and R. Owen, "Large high-performance fast steering mirrors with fpga-embedded controls," *Proc. of SPIE*, vol. 7466, pp. 1–10, 2009.
[57] S. Shao, Z. Tian, S. Song, and M. Xu, "Two-degrees-of-freedom piezo-driven fast steering mirror with cross-axis decoupling capability," *Review of Scientific Instruments*, vol. 89, no. 5, p. 055003, 2018.
[58] H. Langenbach and M. Schmid, "Fast steering mirror for laser communication," in *Proceedings of the 11th ESMATS Symposium*. ESA, 2005.
[59] T. Kentischer, A. Bernert, L. Gantzert, T. Schelenz, and W. Schmidt, "A fast tracking mirror for adaptive optics," *Astrophysics and Space Science*, vol. 239, pp. 213–219, 1996.
[60] Z. Dong, A. Jiang, Y. Dai, and J. Xue, "Space-qualified fast steering mirror for an image stabilization system of space astronomical telescopes," *Applied Optics*, vol. 57, no. 31, pp. 9307–9315, 2018.
[61] R. LeLetty, F. Barillot, H. Fabbro, F. Claeyssen, P. Guay, and L. Cadiergues, "Miniature piezo mechanisms for optical and space applications," *9th International Conference on New Actuators, Bremen, Germany*, 2004.
[62] H. Marth and M. Donat, "Latest experience in design of piezoelectric driven fine steering mirrors," *SPIE Vol. 1543 Active and Adaptive Optical Components*, pp. 248–257, 1991.
[63] S. Xiang, S. Chen, X. Wu, D. Xiao, and X. Zheng, "Study on fast linear scanning for a new laser scanner," *Optics & Laser Technology*, vol. 42, no. 1, pp. 42–46, Feb 2010.
[64] C. Wei, C. Sihai, W. Xin, and L. Dong, "A new two-dimensional fast steering mirror based on piezoelectric actuators," *4th IEEE International Conference on Information Science and Technology*, pp. 308–311, 2014.
[65] S. Kuiper, W. Crowcombe, J. Human, B. Dekker, E. Nieuwkoop, A. Meskers, and W. van der Hoogt, "High bandwidth and compact fine steering mirror development for laser communications," *17the European space mechanisms and tribology symposium*, 2018.
[66] G. Shen, A. Gayhart, D. Eaton, E. Kaelber, and W. Zukowski, "Large angle fast steering mirrors," *SPIE Vol. 1543 Active and Adaptive Optical Components*, pp. 286–293, 1991.

Ernst Csencsics is postdoctoral researcher in the Advanced Mechatronic Systems Lab at the Automation and Control Institute (ACIN) of TU Wien. He received an MSc. and a PhD degree (sub auspiciis) in Electrical Engineering from TU Vienna, Austria in 2014 and 2017, respectively. His primary research interests are on high performance mechatronic systems, the development of holistic methods for multidisciplinary system design and integration, opto-mechatronic measurement and imaging systems, precision engineering, and robot-based in-line measurement systems.

He received the journal best paper award of IEEE/ASME Transactions on Mechatronics (2018) and the best student paper award at the American Control Conference (2016).

Georg Schitter is Professor for Advanced Mechatronic Systems at the Automation and Control Institute (ACIN) of TU Wien. He received an MSc in Electrical Engineering from TU Graz, Austria (2000) and an MSc and PhD degree from ETH Zurich, Switzerland (2004). His primary research interests are on high-performance mechatronic systems, particularly for applications in the high-tech industry, scientific instrumentation, and mechatronic imaging systems, such as AFM, scanning laser and LIDAR systems, telescope systems, adaptive optics, and lithography systems for semiconductor industry.

He received the journal best paper award of IEEE/ASME Transactions on Mechatronics (2018), of the IFAC Mechatronics (2008-2010), of the Asian Journal of Control (2004-2005), and the 2013 IFAC Mechatronics Young Researcher Award. He served as an Associate Editor for IFAC Mechatronics, Control Engineering Practice, and for the IEEE Transactions on Mechatronics.

Post-print version of the article: E. Csencsics and G. Schitter, "Exploring the Pareto Fronts of Actuation Technologies for High Performance Mechatronic Systems," *IEEE Transactions on Mechatronics*, in press, 2020. DOI: 10.1109/TMECH.2020.3016087